



**Secondary ice production in summer clouds over the Antarctic coast:
an underappreciated process in atmospheric models**

Georgia Sotiropoulou^{1,2}, Etienne Vignon³, Gillian Young⁴, Hugh Morrison^{5,6}, Sebastian J.
5 O'Shea⁷, Thomas Lachlan-Cope⁸, Alexis Berne³, Athanasios Nenes^{1,9}

¹Laboratory of Atmospheric Processes and their Impacts (LAPI), Ecole Polytechnique
Fédérale de Lausanne (EPFL), Lausanne, Switzerland

²Department of Meteorology, Stockholm University & Bolin Center for Climate Research,
10 Sweden

³Environmental Remote Sensing Laboratory (LTE), EPFL, Lausanne, Switzerland

⁴School of Earth and Environment, University of Leeds, UK

⁵National Center for Atmospheric Research, Boulder, CO, USA

⁶ARC Centre for Excellence in Climate System Science, University of New South Wales,
15 Sydney, Australia

⁷Centre for Atmospheric Science, University of Manchester, UK

⁸British Antarctic Survey, Cambridge, UK

⁹ICE-HT, Foundation for Research and Technology Hellas (FORTH), Patras, Greece

20 *Correspondence to:* georgia.sotiropoulou@epfl.ch, athanasios.nenes@epfl.ch

Abstract

The correct representation of Antarctic clouds in atmospheric models is crucial for accurate
projections of the future Antarctic climate. This is particularly true for summer clouds which
25 play a critical role in the surface melting of the ice-shelf in the vicinity of Weddell Sea.
However these clouds are often poorly represented, as ice crystal number concentrations
(ICNCs) are underpredicted by atmospheric models, even when primary ice formation is
constrained with aerosol measurements. Rime-splintering, thought to be the dominant
secondary ice production (SIP) mechanism at temperatures between -8 and -3°C, is also very
30 weak in summer Antarctic conditions. Including a parameterization for SIP due to break-up
(BR) from collisions between ice particles in the Weather and Research Forecasting model
bridges the gap between observations and simulations, suggesting that BR could account for
the enhanced ICNCs in the pristine Antarctic atmosphere. These results are insensitive to
uncertainties in primary ice production. The BR mechanism is currently not represented in



35 most weather prediction and climate models; including this process can have a significant
impact on the Antarctic radiation budget and thus in projections of the future regional climate.

1. Introduction

Predictions of Antarctic climate are hampered by the poor representation of mixed-phase
clouds over the Southern Ocean and the Antarctic Seas (Haynes et al., 2011; Flato et al.,
40 2013; Bodas-Salcedo et al., 2014; Hyder et al., 2018). Model simulations reveal significant
discrepancies in the Antarctic surface radiation budget, associated with cloud biases that are
driven by errors in the representation of the cloud microphysical structure (Lawson and
Gettelman, 2014; King et al., 2015; Listowski and Lachlan-Cope, 2017). A correct
representation of the cloud radiative impacts largely depends on the parameterization of cloud
45 microphysical processes (Listowski and Lachlan-Cope, 2017; Hines et al., 2019; Young et al.,
2019) and precipitation (Vignon et al., 2019), which determine the concentration and
characteristics of liquid drops and ice crystals.

Droplet formation processes are relatively well understood and prediction biases are
known to arise from errors in cloud dynamics and aerosol predictions (Sullivan et al., 2016).
50 Errors in ice formation processes, however, are far from resolved. While progress has been
made during the past decade in the study of primary ice production (DeMott et al., 2011),
secondary ice production (SIP) remains poorly understood (Field et al., 2017). SIP refers to
the generation of ice crystals in a cloud that does not require ice-nucleating particles (INPs)
(Field et al., 2017) and has been studied primarily in convective clouds (Lawson et al., 2015;
55 Field et al., 2017), where the observed ice crystal concentrations (ICNCs) can be up to 3-4
orders of magnitudes higher than the available INPs. However, observations indicate that SIP
can also magnify ICNCs to a significant extent in polar clouds (Lloyd et al., 2015; Lachlan-
Cope et al., 2016) where low aerosol concentrations are frequently found (Lachlan-Cope et
al., 2016; O'Shea et al. 2017), with important implications for the surface radiative balance
60 (Young et al., 2019). Yet the mechanisms underlying SIP remain uncertain (Field et al.,
2017).

The only well-established SIP mechanism that has been extensively implemented in
weather forecast and climate models is rime-splintering (Hallett and Mossop, 1974), also
known as the Hallett-Mossop process (H-M), which refers to the production of ice splinters
65 after collisions of supercooled droplets with ice particles (Hallett and Mossop, 1974;
Heymsfield and Mossop, 1984). This process is effective only in a limited temperature range,
between -8 and -3°C, and requires the presence of supercooled liquid droplets both smaller



and larger than 13 μm and 24 μm , respectively. (Mossop and Hallett, 1974; Choulaton et al., 1980). However, recent studies have shown that H-M cannot sufficiently explain the
70 enhanced ICNCs observed in both Arctic (Sotiropoulou et al., 2020) and Antarctic (Young et al., 2019) clouds. While some Antarctic studies (Vergara-Temprado et al., 2018; Young et al., 2019) suggest that the underestimation of ice multiplication in models might be related to uncertainties in the description of the H-M process, we argue that this is likely driven by the fact that almost no models include other SIP mechanisms.

75 Another SIP mechanism, identified in recent laboratory studies (Leisner et al., 2014; Lauber et al., 2018), is the generation of ice fragments from shattering of relatively large frozen drops. This process however, while it is very efficient in convective clouds (Korolev et al., 2019), it has been found ineffective in polar regions (Fu et al., 2019; Sotiropoulou et al., 2020). This is in agreement with Lawson et al. (2017) and Sullivan et al. (2018a) who have
80 shown that drop-shattering occurs in clouds with a relatively warm cloud base.

Mechanical break-up (BR) of ice particles that collide with each other is another process that results in ice multiplication (Vardiman, 1978; Takahashi et al., 1995) and it operates over a wide temperature range with maximum efficiency around -15°C . Limited knowledge of the BR mechanism comes from few laboratory experiments (Vardiman, 1978;
85 Takahashi et al., 1995) and small-scale modeling (Fridlind et al., 2007; Yano and Phillips, 2011, 2016; Phillips et al., 2017a,b; Sullivan et al., 2018a; Sotiropoulou et al., 2020). To the authors knowledge only two attempts have been made to incorporate this process in mesoscale models (Sullivan et al., 2018b; Hoarau et al., 2018). Specifically, Hoarau et al. (2018) assumed a constant number of fragments (F_{BR}) generated per snow-graupel collision in
90 Meso-NH model, while Sullivan et al. (2018b) implemented a temperature-dependent relationship for F_{BR} in COSMO-ART for several types of collisions (e.g. crystal-graupel, graupel-hail, etc), based on the results of Takahashi et al. (1995). Phillips et al. (2017a) recently developed a physically-based description of F_{BR} , which is a function of collisional kinetic energy and accounts for the effect of the colliding particles' size and rimed fraction
95 (Ψ). While being more advanced than any other parameterization proposed for BR, this scheme has never been implemented in mesoscale models before; it has only been tested in small-scale models for convective (Phillips et al., 2017b; Qu et al., 2020) and Arctic (Sotiropoulou et al., 2020) cloud conditions.

Sotiropoulou et al. (2020) recently showed that the observed ICNCs in Arctic clouds
100 within the H-M temperature zone can be explained only by the combination of BR with the H-M process, which results in a 10 to 20-fold enhancement of the primary ice crystals. Based



on their results, we postulate that BR may also play a critical role in Antarctic clouds and can potentially explain the discrepancy between the observed INPs and ICNCs in the region (Young et al., 2019). To test this hypothesis, we implement parameterizations of the BR process in the Morrison microphysics scheme (Morrison et al., 2005) (hereafter M05) in the Weather and Research Forecasting (WRF) model V4.0.1 and examine their influence on the Antarctic clouds observed during the Microphysics of Antarctic Clouds (MAC) flight campaign (O’Shea et al., 2017; Young et al., 2019).

110 2. Observations

2.1. MAC Instrumentation

The MAC flight campaign was conducted in November–December 2015 over coastal Antarctica and the Weddell Sea, with the aim to offer detailed measurements of the microphysical and aerosol properties of the Antarctic atmosphere. MAC included an extensive suite of airborne and ground-based instruments, a detailed description of which can be found in O’Shea et al. (2017); here we only offer a brief recap of the instrumentation used in this study.

Cloud particle size distributions were derived using the images from two optical array probes (OAPs): a 2D Stereo (2DS, SPEC Inc., USA; Lawson et al., 2006) with a nominal size range of 10 to 1280 μm (10 μm pixel resolution) and a cloud imaging probe (CIP-25, DMT Inc., USA; Baumgardner et al., 2001) with a size range of 25 to 1600 μm . Shattering effect in the probes’ inlet were corrected by applying “antishatter” tips (Korolev et al., 2011) and inter-arrival time (IAT) post analysis (Crosier et al., 2011).

Aerosol particle measurements of sizes 0.25 to 32 μm were made using the Grimm optical particle counter (GRIMM model 1.109), while a Cloud Aerosol Spectrometer (CAS, DMT; Baumgardner et al., 2001; Glen and Brooks, 2013) measured particles between 0.6 to 50 μm . Following the methodology of Young et al. (2019) and O’Shea et al. (2017), we only consider Grimm measurements of particles with diameter smaller than 1.6 μm in our analysis to avoid including data subject to inlet losses at larger particle sizes. Finally, the aircraft also included instrumentation to measure temperature, turbulence, humidity, radiation and surface temperature (King et al., 2008).

2.2 Case study

135 For our investigations we focus on the MAC case examined in Young et al. (2019), for which



they showed that the H-M process, as currently parameterized in WRF, cannot explain the observed ICNCs. Young et al. (2019) utilized measurements from two MAC flights, M218 and M219, combined in one case study; both flights were conducted on 27 November 2015 over the Weddell Sea (Fig. 1): M218 between 15.3-16.7 UTC and M219 between 20.45-22.5
140 UTC. On that day, a low pressure system persisted over the eastern Weddell Sea, resulting in a southeasterly flow reaching the aircraft with air mass back trajectories from around the low pressure system, towards the Antarctic Peninsula and southern Patagonia (O'Shea et al., 2017).

The temperature and microphysical conditions encountered during these flights are
145 representative of the MAC campaign (see Table 1 in O'Shea et al., 2017, and Fig. S6 in Young et al., 2019) and generally representative of West Antarctica (Lachlan-Cope et al., 2016). Cloud measurements were collected mainly within the lowest 1.1 km above sea-level (a.s.l.) during both flights and within a temperature range of ~ -9 to -3°C . Aerosol measurements were consistently low (Young et al., 2019), while ICNCs were substantially
150 higher: the mean concentration of aerosols with sizes between 0.5-1.6 μm was 0.56 scm^{-3} and 0.41 scm^{-3} (cm^{-3} at standard temperature and pressure) for M218 and M219, respectively, while the corresponding mean (max) ICNCs were 1.16 (9.03) L^{-1} and 3.33 (87.31) L^{-1} for the two flights. Such low aerosol conditions and concurrent high ICNC concentrations within this temperature range are frequently found in West Antarctica (Lachlan-Cope et al., 2016).
155 Moreover, similar cloud droplet concentrations (N_{drop}) were measured during both flights (Young et al., 2019): the mean N_{drop} was 82.7 cm^{-3} for M218 and 100.4 cm^{-3} for M219, which are comparable with previous observations from the Antarctic Peninsula (Lachlan-Cope et al., 2016).

160 3. Modeling Methods

3.1. Model set-up

This study is conducted with the WRF model (Skamarock et al., 2008), version 4.0.1, by applying the same model set-up as in Young et al. (2019). Two domains with a respective
165 horizontal resolution of 5 km and 1 km are used, where the inner one is two-way nested to the parent domain (Fig. 1). The polar stereographic projection is applied. The outer domain is centered at 74.2°N , 30°E and includes 201×201 grid points, while the second domain consists of 326×406 grids. Both domains have a high vertical resolution with 70 eta levels, 25 of which correspond to lowest 2 km of the atmosphere. The model top is set to 50 hPa. The



170 simulation period spans from 26 to 28 November 2014, 00:00 UTC, allowing for a 24-hour
spin up period before the day of interest (27 November). The model timestep is set to 30 (6)
sec for the outer (inner) domain, while output data are produced every 30 minutes.

Input data for the initial, lateral and boundary conditions for the simulations are
obtained from the European Centre for Medium-Range Weather Forecasting reanalysis (Dee
175 et al., 2011), as recommended by Bromwich et al. (2013). For both shortwave and longwave
radiation components, the RRTMG radiation scheme (Rapid Radiative Transfer Model for
GCMs) is applied. The Mellor-Yamada-Nakanishi-Niino (MYNN; Nakanishi and Niino,
2006) 2.5-level closure planetary boundary layer (PBL) and surface options are also
implemented, in combination with the Noah Land Surface Model (Noah LSM; Chen and
180 Dudhia, 2001), which includes a simplified thermodynamic sea-ice model. Given the short
run length, time-varying sea ice concentrations are not utilized. Young et al. (2019) used the
PWRP V3.6.1 to represent fractional sea-ice, a capability not available in standard WRF
V3.6. However, this option has been made available in the more recent V4.0.1 that we use in
this study. Following Young et al. (2019), the sea-ice albedo is set to 0.82, with a default
185 thickness of 3 m, and snow accumulation depth on sea ice is allowed to vary between 0.001m
and 1.0 m.

Cumulus parameterization is neglected in both domains to ensure all cloud processes
are represented by the grid-scale microphysics scheme. Note that 5 km is a general upper limit
for a convection-resolving resolution (Klemp, 2006; Prein et al., 2015). Cloud microphysics
190 are parameterized following Morrison et al. (2005), hereafter M05. M05 performs well in
reproducing Antarctic clouds, resulting in improved representation of the liquid phase and
thus the cloud radiative effects (Listowski and Lachlan-Cope, 2017; Hines et al., 2019). This
bulk microphysics scheme predicts mixing ratios and number concentrations for cloud water,
cloud ice, rain, snow and graupel. N_{drop} is, however, specified. The default value of the
195 scheme is 200 cm^{-3} ; here N_{drop} is set to 92 cm^{-3} , which is the mean value of M218 and M219
flight measurements (see Section 2.2).

3.2 Sensitivity Simulations

A detailed description of the ice formation processes in M05 and the implemented BR
200 parameterizations is offered in Appendix A and B, respectively. We assume that collisions
that include at least one large particle (thus ice-snow, ice-graupel and graupel-snow, snow-
snow and graupel-graupel) result in ice multiplication; contribution from collisions between
small ice particles (cloud ice) are neglected. Additionally to the control (CNTRL) simulation,



which corresponds to the default set-up of M05, we perform seven sensitivity simulations
205 with varying description of F_{BR} .

In two sensitivity simulations we assume, as in Hoarau et al. (2018), a constant
number of fragments generated per collision. This number is constrained by in-situ
measurements from the Arctic (Schwarzenboeck et al., 2009) which indicated that one-branch
ice-crystals are more common in polar clouds, resulting in ejection of a single fragment after
210 collision with another ice particle; however this analysis (Schwarzenboeck et al., 2009)
included only dendritic crystals with size larger than 300 μm . Based on these results we
perform two simulations: FRAG1 assumes all collision types generate one fragment without
any size restrictions, while FRAG1siz allows for ice multiplication only if the particle that
undergoes fragmentation is larger than 300 μm . Note that since the separation size between
215 ice and snow in the M05 scheme is 125 μm , collisions that include cloud ice do not result in
any multiplication in FRAG1siz.

The standard temperature-dependent formula of Takahashi et al. (1995) for F_{BR} ,
applied in Sullivan et al. (2018b), is tested here in the TAKAH simulation. However,
Takahashi et al. (1995) used 2-cm hailballs in their experiments, which is an unrealistic set-
220 up. For this reason we perform an additional simulation, TAKAHsiz, in which this
relationship is further scaled with size (see Appendix B). Finally, the Phillips
parameterization is implemented in three simulations with varying Ψ for the cloud ice/snow
particles that undergo fragmentation; Ψ is not predicted in most bulk microphysics scheme,
including M05, and thus it is prescribed as a constant. These simulations are referred as
225 PHIL0.2, PHIL0.3 and PHIL0.4 in the text, where the number indicates the assumed values of
 Ψ .

4. Results

230 4.1 BR effect on microphysical properties

In Fig. 2a the modeled total ice number concentrations (cloud ice + snow + graupel, N_{isg})
derived for the region encompassing the 2 MAC flights (Fig. 1) are compared with
measurements derived from the 2D Stereo (2DS) probe (see Section 2.1 for details). Since
2DS cannot detect ice particles smaller than 80 μm , only modeled ice particles with sizes
235 larger than this threshold are considered in this figure, like in Young et al. (2019). While
mean and maximum statistics are discussed below, additional statistical metrics (e.g. median
and interquartile range) are shown in Fig. S1 (Text S1). The mean observed N_{isg} for the whole



MAC campaign generally fluctuates between $0.5\text{--}4\text{ L}^{-1}$. The variation in N_{isg} with temperature is somewhat larger for our case study (November 27), as maximum mean concentration goes up to $\sim 7\text{ L}^{-1}$ at $T = -6.5^\circ\text{C}$. The CNTRL simulation consistently underestimates the mean observations, as it produces mean $N_{\text{isg}} \sim 0.1\text{ L}^{-1}$ over the examined temperature range (Fig. 2a).

PHIL0.2 and PHIL0.3 produce similar results to CNTRL (Fig. 2a, b), suggesting that lightly to moderately rimed ice particles do not contribute to ice multiplication through collisional break-up. The higher rimed fraction in PHIL0.4 results in very good agreement with mean observations (Fig. 2a), especially over the whole MAC case. FRAG1siz is also close to mean observations, but when the size restrictions are ignored (FRAG1) the model gives substantial ICNC overestimation. TAKAH simulation also produces unrealistically high mean N_{isg} , while TAKAHsiz is in closer agreement with observations. The largest deviations from observations for TAKAHsiz are observed for temperatures below -7°C ; however the case study lacks good measurement statistics at this temperature range, since very few observations are available (Fig. 2a).

Overall, CNTRL, PHIL0.2 and PHIL0.3 cannot reproduce the observed spectrum (Fig. 2b). PHIL0.4, FRAG1siz and TAKAHsiz, however, can successfully reproduce the observed range of values (Fig. 2b), but their relative frequency remains underestimated for ICNCs larger than 0.5 L^{-1} . FRAG1 is in closest agreement with the observed spectrum, while TAKAH often overestimates the relative frequency (Fig. 2b). Maximum ICNCs in FRAG1 and TAKAH are 6403 and 2600 L^{-1} , respectively, which are about 70 and 30 times larger than the observed maximum value: 88 L^{-1} . This suggests that BR parameterizations that do not account for the impact of size are rather unrealistic. The maximum ICNCs in PHIL0.4, FRAG1siz and TAKAHsiz are 174 L^{-1} , 150 L^{-1} and 173 L^{-1} , which agree to within a factor of two with observations, while they are substantially underestimated in CNTRL (7.8 L^{-1}), PHIL0.2 (4.7 L^{-1}) and PHIL0.3 (5.2 L^{-1}).

Vertical distributions of cloud ice (N_i), graupel (N_g) and snow (N_s) number concentration are examined in Fig. 3(a-c) for all simulations except those that produce unrealistically large concentrations (FRAG1 and TAKAH). The observed ICNCs are also shown in Fig. 3a and 3c; for consistency with M05, the threshold size separating measured cloud ice from snow is set to $125\text{ }\mu\text{m}$. Graupel concentrations cannot be distinguished in the measurements (hence no ‘Nov 27’ profile in Fig. 3b), however the more realistic model simulations suggest that these are negligible compared to cloud ice/snow concentrations.

PHIL0.2 and PHIL0.3 produce slightly larger N_i (Fig. 3a) than CNTRL, but reduced N_g (Fig. 3b) values and similar or reduced N_s (Fig. 3c); all these mean N_i and N_s profiles are



orders of magnitude lower than the observed values. PHIL0.4, FRAG1siz and TAKAHsiz produce somewhat larger N_i than the observations (Fig. 3a), while N_s is somewhat underestimated (Fig. 3c). FRAG1siz is in slightly better agreement with N_i observations than the other two simulations, especially at heights above 750 m a.s.l (Fig. 3a). Activating BR generally results in reduction of N_g (Fig. 3b). This decrease is larger than one order of magnitude in the three realistic simulations, compared to CNTRL, however we cannot assess which of these graupel profiles better represents reality. Nevertheless, we can overall conclude that PHIL0.4, FRAG1siz and TAKAHsiz result in improved agreement of the vertical distribution of total ICNCs with observations compared to the rest of the simulations, including the default set-up of M05.

The simulated liquid water content (LWC) is compared with CAS observations in Fig. 4. All simulations, except TAKAH, produce similar or slightly overestimated mean LWC at temperatures $\leq -3.5^\circ\text{C}$; at -3°C the mean observed values are higher (Fig. 4a). An overestimation of LWC in these runs is more evident in Fig. 4b; the observed spectrum does not include values larger than 0.5 g m^{-2} , while the simulated spectra are wider. An exception to this is TAKAH simulation, which underestimates mean LWCs and glaciates clouds at temperatures below -7°C (Fig. 4a), while it produces a narrower LWC spectrum compared to the observed (Fig. 4b). Apart from TAKAH, the rest of the simulations produce similar liquid water properties with minor improvements in the runs with reduced LWC values, e.g. in FRAG1 (Fig. 4a). Nevertheless, while the produced range of LWC values in FRAG1 is somewhat closer to the observed, it still underestimates the relative frequency for most of the observed spectrum (Fig. 4b).

4.2 BR effect on surface radiation

To examine how deviations in ICNCs affect climate, mean radiative fluxes at the surface and at the top of the atmosphere (TOA) for all model simulations are presented in Table 1. Increasing BR multiplication has a pronounced impact on shortwave radiation, as it results in decreasing sunlight reflection and thus increasing downward surface radiation (SWD_{SFC}). Upward surface radiation (SWU_{SFC}) is a function of SWD and thus exhibits similar behaviour. This is due to the fact that increased BR efficiency (Fig. 2) results in decreased liquid water path (LWP). However, no substantial differences in mean cloud optical thickness are indicated for CNTRL (40.1 g m^{-2}), PHIL0.2 (33.2 g m^{-2}), PHIL0.3 (40.2 g m^{-2}), PHIL0.4 (29.1 g m^{-2}) and FRAG1siz (30.1 g m^{-2}), which have a mean LWP almost within the black body emission range (Stephens, 1978). Optically thinner clouds are produced in TAKAHsiz



(23.1 g m⁻²), and especially in FRAG1 (8.2 g m⁻²) and TAKAH (3.2 g m⁻²) runs. Note that most simulations, including CNTRL, produce wider LWC spectra than the observed, by overestimating cloud liquid (Fig. 4b). Generally, decreasing liquid content is in better agreement with observations (see section 4.1), suggesting that including the BR process in
310 M05 likely shifts the simulated LWPs towards more realistic values. However, excessive ice multiplication, as in TAKAH, results in unrealistic liquid properties (Fig. 4a) and thus errors in surface radiation.

The difference between CNTRL and the simulations that improve ICNC representation (PHIL0.4, FRAG1siz and TAKAHsiz) fluctuates between 11.9-25.7 Wm⁻² for
315 SWD_{SFC} and 6.7-12.4 Wm⁻² for SWU_{SFC} (Table 1). Pronounced reduction in downward longwave surface radiation (LWD_{SFC}) is only found for the simulations FRAG1siz, FRAG1 and TAKAHsiz, which have a mean LWP well below 30 g m⁻², the lowest limit of the black body emission range (Stephens, 1978). In all other simulations, the reduction in cloud liquid due to BR is not large enough to alter the cloud emissivity significantly. The upward
320 longwave component (LWU_{SFC}) is only slightly affected in all simulations (<~ 1.3 Wm⁻²). Young et al. (2019) showed that underestimation of ICNCs results in significant both positive and negative biases in the surface Cloud Radiative Forcing (CRF) over the coastal areas; our results agree with their findings, as CRF biases vary between -78 Wm⁻² and +86 Wm⁻² for the most realistic simulations (Fig. S2, Text S2). Furthermore, the difference between CNTRL
325 and the realistic simulations in upward radiation flux at TOA (Table 1) is also more pronounced for the shortwave component (SWU_{TOA}), fluctuating between 4.7-9.2 Wm⁻², and less significant for LWU_{TOA} (1.4-3.6 Wm⁻²). All in all, both surface and TOA radiation results indicate that a correct representation of SIP in the atmospheric models is critical for the projection of the energy budget and thus for the future Antarctic climate.

330

4.3 Sensitivity to uncertainties in H-M and primary ice production

The accuracy of SIP representation strongly depends on the uncertainties in the H-M description. To investigate this aspect we allow for a more efficient H-M process that is active over the whole droplet size spectrum (Fig. S3, Text S3). While this modification is not in
335 agreement with the current knowledge on the H-M mechanism derived from laboratory studies (Hallet and Mossop, 1974; Choulaton et al., 1980), it has been applied in previous modeling studies (Sinclair et al., 2016; Young et al., 2019) resulting in improved representation of the cloud ice properties. However, in these additional sensitivity tests the H-M process remains very weak and cannot explain the observed concentrations, if BR is not



340 accounted for in the simulations. The BR mechanism, on the other hand, can explain the
observed ICNCs even when H-M is deactivated (Fig. S3).

BR efficiency can be largely affected by the uncertainty in primary ice production,
which e.g. is a factor of 10 in the applied deposition/condensation-freezing nucleation scheme
(DeMott et al., 2010). Additional sensitivity tests with the Phillips parameterization for
345 collisional break-up indicate that decreasing the efficiency of all primary ice production
mechanisms by a factor of 10 inhibits BR multiplication (Fig. S4, Text S4). Increasing
primary ice production by the same factor in CNTRL still results in substantially
underestimated ice concentrations than the observed (Fig. S4) if BR is not accounted for,
providing additional evidence for the significant role of SIP in these conditions. Activating
350 BR in these high INP conditions produces similar ICNCs as when the standard primary ice
production mechanisms are employed. These findings suggest that BR is not very sensitive to
uncertainties in primary ice production, as long as there are enough primary ice crystals to
initiate this process.

355 **5. Conclusions**

Our results indicate that collisional break-up can explain observations of enhanced ICNCs in
coastal Antarctic clouds, in which primary ice nucleation and H-M efficiency are limited. The
studied case is representative for summer low-level clouds in West Antarctica, which is the
region where large discrepancies between INPs and ICNCs are known to occur within the
360 examined temperature range (Lachlan-Cope et al., 2016; O'Shea et al., 2017). The
conclusions may not hold for winter clouds in the region, which contain less supercooled
liquid water (Listowski et al., 2019) and are less prone to riming, and thus may not favour
BR. Nevertheless, summer clouds play a critical role in the surface melting of the ice-shelf in
the vicinity of Weddell Sea (Gilbert et al., 2020) in West Antarctica and thus their accurate
365 microphysical representation in models is of great importance.

Although BR has been observed in polar conditions before (Rangno and Hobbs, 2001;
Schwarzenboeck et al., 2009), this mechanism is currently not implemented in most weather
prediction and climate models. The more advanced Phillips parameterization produces
realistic ICNCs in Antarctic clouds, as long as a high rimed fraction is prescribed for the
370 particles that undergo fracture, in agreement with Sotiropoulou et al. (2020). A comparison of
vapor deposition rates with riming rates (which include mass changes due to collisions with
droplets/raindrops and due to contact/immersion freezing) for CNTRL simulation indicate
that these two are on average comparable for cloud ice, while riming rates are substantially



larger than vapor deposition rates for snow (not shown). These results indicate that
375 prescribing a high rimed fraction for cloud ice and snow in M05 is not unreasonable;
nevertheless Ψ in reality is highly variable for different temperature and microphysical
conditions. More simplified parameterizations also produce improved results as long as the
impact of the dependence of F_{BR} on the ice particle size is accounted for.

The very few existing BR descriptions in mesoscale models either do not account for
380 size limitations (Sullivan et al., 2018b) or do not account for all collision types (Hoarau et al.,
2018), which limits their realism. Increasing ICNCs from BR alters significantly the radiative
effects of summer Antarctic clouds, suggesting that an accurate representation of this process
in models can impact the future projection of regional climate.

385 **Appendix A: Ice formation processes in M05 scheme**

The standard M05 scheme includes three primary ice production mechanisms (immersion
freezing, contact freezing and deposition/condensation-freezing nucleation), and one SIP
process (H-M). Immersion freezing of cloud droplets and rain is parameterized after Bigg
(1953). This mechanism is active below -4°C and produces a raindrop freezing rate that
390 depends on the degree of supercooling and the number concentration and volume of
supercooled drops. Meyers et al. (1992) description is used for contact freezing, also active
below -4°C , but the rates are further weighted by the effective diffusivity of the contact
nuclei.

The default parameterization for deposition/condensation-freezing ice nucleation in
395 M05 is Cooper (1986), which depends only on temperature and is active below -8°C in liquid
saturated conditions or when ice supersaturation exceeds 8%. However, the DeMott et al.
(2010) parameterization for heterogeneous nucleation has been shown to compare better with
in-cloud ice measurements over the Antarctic Peninsula than Cooper (Listowski and Lachlan-
Cope, 2017). For this reason, we apply the DeMott description in our simulations, where the
400 mean aerosol concentration of particles with sizes between $0.5\text{-}1.6\ \mu\text{m}$ for the two flights
($0.49\ \text{scm}^{-3}$) is used as input (Young et al., 2019).

The H-M description, adapted from Reisner et al. (1998), is based on the laboratory
experiments conducted by Hallett and Mossop (1974), who found a maximum of ~ 350
splinters per milligram of rime generated around -5°C :

$$405 \quad \frac{dN_{iHM}}{dt} = \rho \cdot 3.5 \cdot 10^8 f(T) \frac{dm_{rime}}{dt} \quad (1)$$

where dN_{iHM}/dt is the number of new fragments produced at a given timestep, $f(T)$ is the



temperature-dependent efficiency of the process, ρ is the air density, and dm_{rime}/dt is the mass production rate of rime on snow or graupel due to accretion of cloud and rain drops. $f(T)$ is 0 for $T < -8^\circ\text{C}$ and $T > -3^\circ\text{C}$, 1 for $T = -5^\circ\text{C}$, and increases linearly between these two extremes for $T \geq -8^\circ\text{C}$ and $T \leq -3^\circ\text{C}$.

Furthermore, for H-M to become activated in M05, two conditions must be met: (a) snow (or graupel) mass mixing ratios must be greater than 0.1 g kg^{-1} and (b) cloud liquid (or rain) water mass mixing ratios should be greater than 0.5 (or 0.1) g kg^{-1} . To achieve a good agreement between modeled and observed ICNCs for the simulated case, Young et al. (2019) had to remove condition (b) and multiply the H-M efficiency by a factor of 10.

Appendix B: Parameterizing collisional break-up in M05

There are three types of ice particles considered in the M05 scheme: small (cloud) ice, snow, and graupel. Ice multiplication is allowed after cloud ice-snow, cloud ice-graupel, graupel-snow, snow-snow and graupel-graupel collisions. The standard M05 scheme includes a description for collisions between cloud ice and snow to represent the accretion process, following the “continuous collection” approach:

$$\frac{dN_{iAC}}{dt} = \frac{\pi}{4} \rho E_{col} \Gamma(b_s + 3) a_s \frac{N_i N_{0s}}{\lambda_s^{(b_s+3)}} \quad (2)$$

dN_{iAC}/dt is the rate of ice crystal number concentration collected by snow. N_{0s} and λ_s are the intercept and slope parameters of the snow size distribution, represented by an inverse exponential function, and Γ is the Euler gamma function. a_s and b_s are the characteristic parameters for snow in the fallspeed-diameter relationship (Morrison et al., 2005); a_s includes a density correction factor (Heymsfield et al., 2007). Note that the diameter (d_i) and terminal velocity (u_i) of cloud ice particles are considered much smaller than those of snow: $d_i \ll d_s$ and $u_i \ll u_s$, so that they are neglected in Eq. (2). E_{col} is the collection (sticking) efficiency between ice particles, set to 0.1; hence, it is assumed that only 10% of cloud ice particles that collide with snow are actually collected. We assume the remaining 90% of collisions result in ice particle break-up, hence the following relationship gives the rate of cloud ice-snow collisions that contribute to ice multiplication:

$$\frac{dN_{iIS}}{dt} = \frac{\pi}{4} \rho (1 - E_{col}) \Gamma(b_s + 3) a_s \frac{N_i N_{0s}}{\lambda_s^{(b_s+3)}} \quad (3)$$

In the default M05, collisions between cloud ice and graupel particles are neglected as it is assumed that the collection efficiency of such collisions is negligible. To represent cloud ice-graupel collisions for ice multiplication, we use Eq. (3), but the size distribution and



fallspeed parameters of snow are replaced by those for graupel. Moreover, since cloud ice is
 440 not collected by graupel particles, we assume that 100% of these collisions result in cloud ice
 break-up:

$$\frac{dN_{ig}}{dt} = \frac{\pi}{4} \rho \Gamma (b_g + 3) a_g \frac{N_i N_{og}}{\lambda_g^{(b_g+3)}} \quad (4)$$

In the default M05 scheme, collisions between snow and graupel are also neglected because it
 is assumed that the collection efficiency for such collisions is negligible. For this study,
 445 graupel-snow collisions are treated using expressions similar to those for raindrop-snow
 collisions in M05. These are adapted from Ikawa and Saito (1991) and represent collisions
 between relatively large precipitation-sized particles:

$$\frac{dQ_{isg}}{dt} = \pi^2 \rho_s \rho \left| \Delta u_{msg} \right| \frac{N_{os} N_{og}}{\lambda_s^3} \left(\frac{5}{\lambda_s^3 \lambda_g} + \frac{2}{\lambda_s^2 \lambda_g^2} + \frac{0.5}{\lambda_s \lambda_g^3} \right) \quad (5)$$

$$\frac{dN_{isg}}{dt} = \frac{\pi}{2} \rho \left| \Delta u_{msg} \right| N_{os} N_{og} \left(\frac{1}{\lambda_s^3 \lambda_g} + \frac{1}{\lambda_s^2 \lambda_g^2} + \frac{1}{\lambda_s \lambda_g^3} \right) \quad (6)$$

450 where $\left| \Delta u_{msg} \right| = \left((1.2u_{ms} - 0.95u_{mg})^2 + 0.08u_{mg}u_{ms} \right)^{1/2}$ (7)

and $\left| \Delta u_{msg} \right| = \left((1.7u_{ns} - u_{ng})^2 + 0.3u_{ng}u_{ns} \right)^{1/2}$ (8)

dQ_{isg}/dt and dN_{isg}/dt represent the bulk rates that snow mass and number concentration
 collide with graupel and contribute to ice multiplication through fragmentation. Corrections in
 the mass (or number) -weighted difference in terminal velocity Δu_{msg} (or Δu_{msg}) of the
 455 colliding particles (Eq. 7,8) are adapted from Mizuno (1990) and Reisner et al. (1998), to
 account for underestimates when $u_{ns} \approx u_{ng}$

M05 also includes a description for collisions between snowflakes to represent snow
 aggregation, following Passarelli (1978):

$$\frac{dN_{sAG}}{dt} = \frac{-1108a_s E_{col}}{4 \times 720} \pi^{\frac{1-b_s}{3}} \rho^{\frac{2+b_s}{3}} \rho_s^{\frac{-2-b_s}{3}} Q_s^{\frac{2+b_s}{3}} N_s^{\frac{4-b_s}{3}} \quad (9)$$

460 Based on this expression we parameterize the number of snow-snow collisions that contribute
 to ice multiplication as:

$$\frac{dN_{iss}}{dt} = \frac{1108a_s(1-E_{col})}{4 \times 720} \pi^{\frac{1-b_s}{3}} \rho^{\frac{2+b_s}{3}} \rho_s^{\frac{-2-b_s}{3}} Q_s^{\frac{2+b_s}{3}} N_s^{\frac{4-b_s}{3}} \quad (10)$$

Because snow aggregation does not result in any mass transfer, the snow mass involved in
 these collisions is not calculated by the default M05 scheme. We obtain a description of dQ_{iss}
 465 $/dt$ by applying the size distribution and fallspeed parameters of snow in the analytical
 solution for self-collection derived by Verlinde et al. (1990):

$$\frac{dQ_{iss}}{dt} = \frac{914\pi^2}{48\rho\rho_s} (1 - E_{col}) a_s d_s^{b_s+5} N_s^2 \quad (11)$$



To test the consistency of Eq. (10) and (11), which were derived using different methods, we repeated the CNTRL and PHIL0.4 simulations but with the Eq. (9) and (10) replaced by the analytical solution for the change in number concentration from self-collection derived by Verlinde and Cotton (1993). The sensitivity of the results to this modification was found to be insignificant.

Graupel-graupel collisions are also parameterized in a similar manner. Since there is no graupel aggregation (collection efficiency of such collisions is assumed to be negligible), 100% of the collisions are assumed to contribute to break-up:

$$\frac{dN_{igg}}{dt} = \frac{1108a_g}{4 \times 720} \pi^{\frac{1-b_g}{3}} \rho^{\frac{2+b_g}{3}} \rho_g^{\frac{-2-b_g}{3}} Q_g^{\frac{2+b_g}{3}} N_g^{\frac{4-b_g}{3}} \quad (12)$$

$$\frac{dQ_{igg}}{dt} = \frac{836\pi^2}{48\rho\rho_g} a_g d_g^{b_g+5} N_g^2 \quad (13)$$

The value 1108 in Eq. (10) is valid for $b_s=0.4$ (Passarelli, 1978); in M05 $b_s=0.41$ and $b_g=0.37$, thus adapting this value for both snow-snow (10) and graupel-graupel (12) collisions is a reasonable approximation.

Following the methodology of Sullivan et al. (2018b) in TAKAH simulation, the number of fragments generated due to ice-ice particle collisions (F_{BR}) is:

$$F_{BR} = 280 (T - 252)^{1.2} e^{-(T-252)/5} \quad (14)$$

However, Takahashi et al. (1995) used 2-cm hailballs in their experiments, thus to further include the influence of size in this formulation, we implement a size-scaled expression in TAKAHsiz simulation, assuming that F_{BR} depends linearly on D , decreasing to 0 at $D = 0$:

$$F_{BR} = 280 (T - 252)^{1.2} e^{-(T-252)/5} \frac{D}{D_o} \quad (15)$$

where D (in meters) is the size of the ice particle that undergoes fracturing and $D_o=0.02$ m, the size of hailballs used by Takahashi et al. (1995).

The Phillips et al. (2017a) parameterization allows for varying treatment of F_{BR} depending on the ice crystal type and habit.

$$F_{BR} = \alpha A \left(1 - \exp \left\{ - \left[\frac{CK_o}{\alpha A} \right]^\psi \right\} \right) \quad (16)$$

$$\text{where : } K_o = \frac{m_1 m_2}{m_1 + m_2} (\Delta u_{n12})^2,$$

$$\psi = 3.5 \times 10^{-3}$$

$$a = \pi D^2$$

m_1, m_2 are the masses of the colliding particles and Δu_{n12} is the difference in their terminal velocities. The correction applied in Eq. (8) is also adapted here to account for underestimates when $u_{n1} \approx u_{n2}$. D (in meters) is the size of the smaller ice particle which undergoes



fracturing and α is its surface area. The parameterization was developed based on particles with diameters $500 \mu\text{m} < D < 5 \text{ mm}$, however Phillips et al. (2017a) suggest that it can be used for particle sizes outside the recommended range as long as the input variables to the scheme are set to the nearest limit of the range. C is the asperity-fragility coefficient and ψ is a correction term for the effects of sublimation based on the field observations by Vardiman (1978). For cloud ice-snow, cloud ice-graupel, snow-graupel and snow-snow collisions:

$$A = 1.58 \cdot 10^7 (1 + 100\Psi^2) \left(1 + \frac{1.33 \cdot 10^{-4}}{D^{1.5}}\right),$$

$$\gamma = 0.5 - 0.25\Psi,$$

$$C = 7.08 \times 10^6 \psi$$

The above parameters adapted from Phillips et al. (2017a) concern planar crystals or snow with rimed fraction $\Psi < 0.5$ that undergo fracturing: $\Psi \leq 0.2$ corresponds to lightly rimed particles, while $\Psi \approx 0.4$ represents highly rimed crystals/snow. The choice of the ice habit is based on particle images collected during the MAC flights, which indicate the presence of needles and planar particles (O'Shea et al., 2017); needles are often considered secondary ice (Field et al., 2017). However, the M05 scheme does not explicitly consider habit and assumes spherical particles for all processes except sedimentation, for which the fallspeed-diameter relationships are for non-spherical ice.

For graupel-graupel collisions the parameters implemented in Eq. (16) are somewhat different (Phillips et al., 2017a):

$$A = \frac{a_o}{3} + \max\left(\frac{2a_o}{3} - \frac{a_o}{9} |T - 258|, 0\right)$$

$$\gamma = 0.3,$$

$$C = 6.3 \times 10^6 \psi$$

Finally, an upper limit for the number of fragments produced per collision is imposed, set to $F_{BRmax} = 100$; this is the same for all collision types (Phillips et al., 2017a).

We estimate the production rate of fragments for cloud ice-snow collisions and cloud ice-graupel collisions using Eq. (3) or (4) and one of the proposed formulations for F_{BR} above: $\frac{dN_{is}}{dt} F_{BR}$ and $\frac{dN_{ig}}{dt} F_{BR}$. For both of these collision types we assume that the cloud ice particles undergo break-up and the new smaller ice fragments remain within the same ice particle category. For snow-graupel collisions, where the snow particle is assumed to undergo fracturing, the production term $\frac{dN_{isg}}{dt} F_{BR}$ is added to the cloud ice category. In this case mass transfer from the snow to the cloud ice category also occurs, but according to Phillips et al. (2017a) this is only 0.1% of the snow mass that collides with graupel (5). Snow-snow and



graupel-graupel collisions are handled in the same way: $\frac{dN_{iss}}{dt} F_{BR}$ and $\frac{dN_{igg}}{dt} F_{BR}$ are added to the cloud ice number equation, while 0.1% of $\frac{dQ_{iss}}{dt}$ (11) and $\frac{dQ_{igg}}{dt}$ (13) is added to the corresponding mass equation.

530

Code and data availability: MAC data are available at <https://catalogue.ceda.ac.uk/uuid/da17dab196f74d64af3ccbc35624027b>. The modified Morrison scheme is available upon request

535 **Competing interests:** The authors declare that they have no conflict of interest.

Author contribution: GS and AN conceived and led this study. EV helped with the model configuration and set-up, and provided Fig. 1. GY provided the observations and the model set-up for the MAC case. SJO post-processed MAC data. GS implemented the BR parameterizations, performed the WRF simulations, analyzed the results and, together with AN, led the manuscript writing. All authors contributed to the scientific interpretation, discussion and writing of the manuscript.

545 **Acknowledgements:** GS and AN acknowledge support from Laboratory of Atmospheric Processes and Their Impacts (LAPI) at the Ecole Polytechnique Federale de Lausanne (EPFL) the project IC-IRIM (project ID 2018-01760) funded by the Swedish Research Council for Sustainable Development (FORMAS), the project PyroTRACH (ERC-2016-COG) funded from H2020-EU.1.1. - Excellent Science - European Research Council (project ID 726165) and the project FORCeS funded from Horizon H2020-EU.3.5.1. (project ID 821205). EV and
550 AB acknowledge the financial support from EPFL-ENAC through the LOSUMEA project. The National Center for Atmospheric Research is sponsored by the U.S. National Science Foundation. We are also grateful to MAC scientific crew for the observational datasets used in this study.

555 **References:**

Baumgardner, D., Jonsson, H., Dawson, W., O'Connor, D., and R. Newton: The cloud, aerosol and precipitation spectrometer: A new instrument for cloud investigations. *Atmos. Res.*, 59, 251–264. [https://doi.org/10.1016/S0169-8095\(01\)00119-3](https://doi.org/10.1016/S0169-8095(01)00119-3), 2001



560

Bodas-Salcedo, A., Williams, K. D., Ringer, M. A., Beau, I., Cole, J. N. S., Dufresne, J.-L., et al.: Origins of the solar radiation biases over the Southern Ocean in CFMIP2 Models, *J. Clim.*, 27, 41–56. <https://doi.org/10.1175/JCLI-D-13-00169.1>, 2014

565 Bigg, E. K. : The formation of atmospheric ice crystals by the freezing of droplets. *Q. J. Roy. Meteorol. Soc.*, 79, 510–519. <https://doi.org/10.1002/qj.49707934207>, 1953

Bromwich, D. H., Otieno, F. O., Hines, K. M., Manning, K.W., and Shilo, E.: Comprehensive evaluation of polar weather research and forecasting model performance in the Antarctic, *Journal of Geophysical Research: Atmospheres*, 118, 274–292, doi:10.1029/2012jd018139, <http://dx.doi.org/10.1029/2012JD018139>, 2013.

Brown, P. and Francis, P.: Improved measurements of the ice water content in cirrus using a total-water probe, *J. Atmos. Ocean. Tech.*, 12, 410–414, 1995.

575

Chen, F., and Dudhia, J.: Coupling an Advanced Land Surface–Hydrology Model with the Penn State– NCAR MM5 Modeling System. Part I: Model Implementation and Sensitivity. *Monthly Weather Rev.*, 129, 569–585, 2001.

580 Choulaton, T. W., D. J. Griggs, B. Y. Humood, and Latham, J. : Laboratory studies of riming, and its relation to ice splinter production. *Quart. J. Roy. Meteor. Soc.*, 106, 367–374, doi:<https://doi.org/10.1002/qj.49710644809>, 1980.

Crosier, J., Choulaton, T. W., Westbrook, C. D., Blyth, A. M., Bower, K. N., Connolly, P. J.,
585 Dearden, C., Gallagher, M. W., Cui, Z., and Nicol, J. C.: Microphysical properties of cold frontal rainbands, *Q. J. Roy. Meteorol. Soc.*, 140, 1257–1268, doi:10.1002/qj.2206, 2013.

Cooper, W.A.: Ice initiation in natural clouds. *Meteorological Monographs*, 21, 29–32. <https://doi.org/10.1175/0065-9401-21.43.29>, 1986

590

Dee, D.P., Uppala, S.M., Simmons, A.J., Berrisford, P., Poli, P., Kobayashi, S., Andrae, U.,
Balmaseda, M.A., Balsamo, G., Bauer, P., Bechtold, P., Beljaars, A.C.M., van de Berg, L.,
Bidlot, J., Bormann, N., Delsol, C., Dragani, R., Fuentes, M., Geer, A.J., Haimberger, L.,



- 595 Healy, S.B., Hersbach, H., Holm, E.V., Isaksen, I., Kalberg, P., Kohler, M., Matricardi, M.,
McNally, A.P., Monge-Sanz, B.M., Morcrette, J.-J., Park, B.-K., Peubey, C., de Rosnay, P.,
Tavolato, C., Thepaut, J.-N., Vitart, F.: The ERA-Interim reanalysis: Configuration and
performance of the data assimilation system, *Q. J. Roy. Meteor. Soc.*, 137, 553–597,
<https://doi.org/10.1002/qj.828>, 2011.
- 600 DeMott, P. J., Prenni, A. J., Liu, X., Kreidenweis, S. M., Petters, M. D., Twohy, C. H.,
Richardson, M. S., Eidhammer, T., and Rogers, D. C.: Predicting global atmospheric ice
nuclei distributions and their impacts on climate, *Proc. Nat. Acad. Sci.*,
[doi:10.1073/pnas.0910818107](https://doi.org/10.1073/pnas.0910818107), 2010.
- 605 DeMott, P.J., O. Möhler, O. Stetzer, G. Vali, Z. Levin, M.D. Petters, M. Murakami, T.
Leisner, U. Bundke, H. Klein, Z.A. Kanji, R. Cotton, H. Jones, S. Benz, M. Brinkmann, D.
Rzesanke, H. Saathoff, M. Nicolet, A. Saito, B. Nillius, H. Bingemer, J. Abbatt, K. Ardon, E.
Ganor, D.G. Georgakopoulos, and C. Saunders, 2011: Resurgence in Ice Nuclei Measurement
Research. *Bull. Amer. Meteor. Soc.*, 92, 1623–
610 1635, <https://doi.org/10.1175/2011BAMS3119.1>
- Field, P., Lawson, P., Brown, G., Lloyd, C., Westbrook, D., Moisseev, A., Miltenberger, A.,
Nenes, A., Blyth, A., Choulaton, T., Connolly, P., Bühl, J., Crosier, J., Cui, Z., Dearden, C.,
DeMott, P., Flossmann, A., Heymsfield, A., Huang, Y., Kalesse, H., Kanji, Z., Korolev, A.,
615 Kirchgassner, A., Lasher-Trapp, S., Leisner, T., McFarquhar, G., Phillips, V., Stith, J., and
Sullivan, S.: Chapter 7: Secondary ice production - current state of the science and
recommendations for the future, *Meteor. Monogr.*, [doi:10.1175/AMSMONOGRAPHS-D-16-
0014.1](https://doi.org/10.1175/AMSMONOGRAPHS-D-16-0014.1), 2017.
- 620 Flato, G., Marotzke, J., Abiodun, B., Braconnot, P., Chou, S., Collins, W., Cox, P., Driouech,
F., Emori, S., Eyring, V., Forest, C., Gleckler, P., Guilyardi, E., Jakob, C., Kattsov, V.,
Reason, C., and Rummukainen, M.: Evaluation of Climate Models. In: *Climate Change 2013:
The Physical Science Basis. Contribution of Working Group I to the Fifth Assessment Report
of the Intergovernmental Panel on Climate Change* [Stocker, T.F., D. Qin, G.-K. Plattner, M.
625 Tignor, S.K. Allen, J. Boschung, A. Nauels, Y. Xia, V. Bex and P.M. Midgley (eds.)], 2013.
- Fridlind, A. M., Ackerman, A. S., McFarquhar, G., Zhang, G., Poellot, M. R., DeMott, P. J.,



630 Prenni, A. J., and Heymsfield, A. J.: Ice properties of single-layer stratocumulus during the Mixed-Phase Arctic Cloud Experiment: 2. Model results., *J. Geophys. Res.*, 112, D24202, <https://doi.org/10.1029/2007JD008646>, 2007.

635 Fu, S., Deng, X., Shupe, M.D., and Huiwen X.: A modelling study of the continuous ice formation in an autumnal Arctic mixed-phase cloud case, *Atmos. Res.*, 228, 77-85, <https://doi.org/10.1016/j.atmosres.2019.05.021>, 2019

Gilbert, E, Orr, A, King, JC, et al. Summertime cloud phase strongly influences surface melting on the Larsen C ice shelf, *Antarctica. Q J R Meteorol Soc.* 2020; 1-16. <https://doi.org/10.1002/qj.3753>

640 Glen, A., and Brooks, S. D.: A new method for measuring optical scattering properties of atmospherically relevant dusts using the Cloud and Aerosol Spectrometer with Polarization (CASPOL). *Atmospheric Chemistry & Physics*, 13, 1345–1356, <https://doi.org/10.5194/acp-13-1345-2013>, 2013

645 Hallett, J. and Mossop, S. C.: Production of secondary ice particles during the riming process, *Nature*, 249, 26–28, doi:10.1038/249026a0, 1974.

650 Haynes, J.M., C. Jakob, W.B. Rossow, G. Tselioudis, and J. Brown: Major Characteristics of Southern Ocean Cloud Regimes and Their Effects on the Energy Budget. *J. Climate*, 24, 5061-5080, <https://doi.org/10.1175/2011JCLI4052.1>, 2011

655 Heymsfield, A.J., A. Bansemer, and C.H. Twohy: Refinements to Ice Particle Mass Dimensional and Terminal Velocity Relationships for Ice Clouds. Part I: Temperature Dependence. *J. Atmos. Sci.*, 64, 1047–1067, <https://doi.org/10.1175/JAS3890.1>, 2007

660 Hines, K. M., Bromwich, D. H., Wang, S.-H., Silber, I., Verlinde, J., and Lubin, D.: Microphysics of summer clouds in central West Antarctica simulated by the Polar Weather Research and Forecasting Model (WRF) and the Antarctic Mesoscale Prediction System (AMPS), *Atmos. Chem. Phys.*, 19, 12431–12454, <https://doi.org/10.5194/acp-19-12431-2019>, 2019.



- 665 Hoarau, T., Pinty, J.-P., and Barthe, C.: A representation of the collisional ice break-up process in the two-moment microphysics LIMA v1.0 scheme of Meso-NH, *Geosci. Model Dev.*, 11, 4269–4289, <https://doi.org/10.5194/gmd-11-4269-2018>, 2018.
- Hyder, P., Edwards, J. M., Allan, R. P., Hewitt, H. T., Bracegirdle, T. J., Gregory, J. M., et al.: Critical Southern Ocean climate model biases traced to atmospheric model cloud errors. *Nature Communications*, 9, 3625. <https://doi.org/10.1038/s41467-018-05634-2>, 2018
- 670 Ikawa, M., and Saito, K.: Description of a Non-hydrostatic Model Developed at the Forecast Research Department of the MR, MRI Tech. Rep. 28, 238 pp, 1991
- King J. C., Gadian, A., Kirchgassner, A., Kuipers, Munneke, P., Lachlan-Cope, T. A., Orr, A., Reijmer, C., van den Broeke, M. R., van Wessem, J. M., and Weeks, M.: Validation of the summertime surface energy budget of Larsen C Ice Shelf (Antarctica) as represented in three high-resolution atmospheric models, *J. Geophys. Res.*, 120, 1335–1347, <https://doi.org/10.1002/2014JD022604>, 2015.
- 675 King, J. C., Lachlan-Cope, T. A., Ladkin, R. S., and Weiss, A.: Airborne Measurements in the Stable Boundary Layer over the Larsen Ice Shelf, Antarctica, *Boundary-Layer Meteorology*, 127, 413–428, doi:10.1007/s10546-008-9271-4, 2008.
- Klemp, J. B.: Advances in the WRF model for convection-resolving forecasting, *Adv. Geosci.*, 7, 25–29, <https://doi.org/10.5194/adgeo-7-25-2006>, 2006.
- 685 Korolev, A. V., Emery, E. F., Strapp, J.W., Cober, S. G., Isaac, G. A., Wasey, M., and Marcotte, D.: Small ice particles in tropospheric clouds: fact or artifact?, *B. Am. Meteorol. Soc.*, 92, 967–973, doi:10.1175/2010BAMS3141.1, 2011.
- 690 Korolev, A., Heckman, I., Wolde, M., Ackerman, A. S., Fridlind, A. M., Ladino, L., Lawson, P., Milbrandt, J., and Williams, E.: A new look at the environmental conditions favorable to secondary ice production, *Atmos. Chem. Phys. Discuss.*, <https://doi.org/10.5194/acp-2019-611>, in review, 2019.
- 695 Lachlan-Cope, T., Listowski, C., and O'Shea, S: The microphysics of clouds over the



- Antarctic peninsula—Part 1: Observations. *Atmos. Chem. Phys.*, 16(24), 15,605–15,617.
<https://doi.org/10.5194/acp-16-15605-2016>, 2016
- 700 Lauber, A., Kiselev, A., Pander, T., Handmann, P., and Leisner, T.: Secondary ice formation during freezing of levitated droplets, *J. Atmos. Sci.*, 75, 2815–2826, <https://doi.org/10.1175/JAS-D-18-0052.1>, 2018.
- Lawson, R. P., O'Connor, D., Zmarzly, P., Weaver, K., Baker, B., Mo, Q., and Jonsson, H. : The 2D-S (Stereo) probe: Design and preliminary tests of a new airborne, high-speed, high-resolution particle imaging probe. *Journal of Atmospheric and Oceanic Technology*, 23, 705 1462–1477. <https://doi.org/10.1175/JTECH1927.1>, 2006
- Lawson, R. P., Woods, S., and Morrison, H.: The microphysics of ice and precipitation development in tropical cumulus clouds, *J. Atm. Sci.*, 72, 2429–2445, doi:10.1175/JAS-D-14-0274.1, 2015.
- 710 Lawson, P., Gurganus, C., Woods, S., and Brientjes, R.: Aircraft observations of cumulus microphysics ranging from the tropics to midlatitudes: implications for a “new” secondary ice process, *J. Atmos. Sci.*, 74, 2899–2920, <https://doi.org/10.1175/JAS-D-17-0033.1>, 2017.
- 715 Leisner, T., Pander, T., Handmann, P., and Kiselev, A.: Secondary ice processes upon heterogeneous freezing of cloud droplets, 14th Conf. on Cloud Physics and Atmospheric Radiation, Amer. Meteor. Soc, Boston, MA, 2014.
- Listowski, C., and Lachlan-Cope, T.: The microphysics of clouds over the antarctic peninsula—Part 2:Modelling aspects within Polar WRF. *Atmos. Chem. Phys.*, 17(17), 720 10,195–10,221. <https://doi.org/10.5194/acp-17-10195-2017>, 2017
- Listowski, C., Delanoë, J., Kirchgaessner, A., Lachlan-Cope, T., and King, J.: Antarctic clouds, supercooled liquid water and mixed phase, investigated with DARDAR: geographical and seasonal variations, *Atmos. Chem. Phys.*, 19, 6771–6808, <https://doi.org/10.5194/acp-19-6771-2019>, 2019.
- 725



Lloyd, G., Choullarton, T. W., Bower, K. N., Crosier, J., Jones, H., Dorsey, J. R., Gallagher, M. W., Connolly, P., Kirchgaessner, A. C. R., and Lachlan-Cope, T.: Observations and
730 comparisons of cloud microphysical properties in spring and summertime Arctic stratocumulus clouds during the ACCACIA campaign, *Atmos. Chem. Phys.*, 15, 3719–3737, <https://doi.org/10.5194/acp-15-3719-2015>, 2015.

Meyers, M. P., DeMott, P. J., and Cotton, W. R.: New primary ice-nucleation
735 parameterizations in an explicit cloud model. *Journal of Applied Meteorology*, 31, 708–721. [https://doi.org/10.1175/1520-0450\(1992\)031<0708:NPINPI>2.0.CO;2](https://doi.org/10.1175/1520-0450(1992)031<0708:NPINPI>2.0.CO;2), 1992

Mizuno, H.: Parameterization of the accretion process between different precipitation
740 elements. *J. Meteor. Soc. Japan*, 57, 273–281, 1990

Mossop, S. C., and Hallett, J.: Ice crystal concentration in cumulus clouds: Influence of the
drop spectrum. *Science*, 186, 632–634. <https://doi.org/10.1126/science.186.4164.632>, 1974.

Mossop, S. C. (1985). Secondary ice particle production during rime growth: The effect of
745 drop size distribution and rimer velocity. *Quart. J. Roy. Meteor. Soc.*, 111(470), 1113–1124. <https://doi.org/10.1002/qj.49711147012>

Morrison, H., Curry, J.A., and Khvorostyanov, V.I.: A New Double-Moment Microphysics
750 Parameterization for Application in Cloud and Climate Models. Part I: Description, *Atmos. Sci.*, 62, 3683–3704 62, 2005

Nakanishi, N., and Niino, H.: An improved Mellor–Yamada level-3 model: Its numerical
755 stability and application to a regional prediction of advection fog. *Boundary-Layer Meteorology*, 119, 397–407, 2006

O’Shea, S. J., Choullarton, T. W., Flynn, M., Bower, K. N., Gallagher, M., Crosier, J., Williams, P., Crawford, I., Fleming, Z. L., Listowski, C., Kirchgaessner, A., Ladkin, R. S., and Lachlan-Cope, T.: In situ measurements of cloud microphysics and aerosol over coastal
760 Antarctica during the MAC campaign, *Atmos. Chem. Phys.*, 17, 13049–13070, <https://doi.org/10.5194/acp-17-13049-2017>, 2017.



Passarelli, R.E.: An Approximate Analytical Model of the Vapor Deposition and Aggregation Growth of Snowflakes., *J. Atmos. Sci.*, 35, 118–124, 1978

765 Phillips, V.T.J., Yano, J.-I., and Khain, A.: Ice multiplication by breakup in ice-ice collisions. Part I: Theoretical formulation, *J. Atmos. Sci.*, 74, 1705–1719, <https://doi.org/10.1175/JAS-D-16-0224.1>, 2017a.

770 Phillips, V.T.J., Yano, J.-I., Formenton, M., Ilotoviz, E., Kanawade, V., Kudzotsa, I., Sun, J., Bansemer, A., Detwiler, A.G., Khain, A., and Tessorod, S.A.: Ice Multiplication by Breakup in Ice–Ice Collisions. Part II: Numerical Simulations. *J. Atmos. Sci.*, 74, 2789–2811, <https://doi.org/10.1175/JAS-D-16-0223.1>, 2017b.

775 Prein, A. F., Langhans, W., Fosser, G., Ferrone, A., Ban, N., Goergen, K., Keller, M., Tille, M., Gutjahr, O., Feser, F., Brisson, E., Kollet, S., Schmidli, J., Lipzig, N. P. M., and Leung, R.: A review on regional convection-permitting climate modeling: Demonstrations, prospects, and challenges, *Reviews of Geophysics*, 53(2), 323–361, [doi:10.1002/2014RG000475](https://doi.org/10.1002/2014RG000475), 2015.

780 Qu, Y., Khain, A., Phillips, V., Ilotoviz, E., Shpund, J., Patade, S., and Chen, B.: The role of ice splintering on microphysics of deep convective clouds forming under different aerosol conditions: Simulations using the model with spectral bin microphysics. *J. Geophys. Res. Atmos.*, 125, e2019JD031312. <https://doi.org/10.1029/2019JD031312>, 2020

785 Rangno, A.L., and Hobbs, P.V., Ice particles in stratiform clouds in the Arctic and possible mechanisms for the production of high ice concentrations, *J. Geophys. Res.*, 106, 15, 065–15,075, 2001.

790 Reisner, J., Rasmussen, R. M., and Bruintjes, R. T.: Explicit forecasting of supercooled liquid water in winter storms using the MM5 mesoscale model, *Quart. J. Roy. Meteor. Soc.*, 124(548), 1071–1107, [doi: 10.1002/qj.49712454804](https://doi.org/10.1002/qj.49712454804), 1998.

Skamarock, W. C., and Klemp, J. B.: A time-split nonhydrostatic atmospheric model for weather research and forecasting applications. *J. Comp. Phys.*, 227(7), 3465–3485. <https://doi.org/10.1016/j.jcp.2007.01.037>, 2008

795



- Schwarzenboeck, A., Shcherbakov, V., Lefevre, R., Gayet, J.-F., Duroure, C., and Pointin, Y.: Indications for stellar-crystal fragmentation in Arctic clouds, *Atmos. Res.*, 92, 220–228, <https://doi.org/10.1016/j.atmosres.2008.10.002>, 2009.
- 800 Sinclair, V.A., Moisseev, D., and Lerber, A.: How dual-polarization radar observations can be used to verify model representation of secondary ice. *J. Geophys. Res.: Atmospheres*, 121, 10, 954–10, 970, 2016
- Sotiropoulou, G., Sullivan, S., Savre, J., Lloyd, G., Lachlan-Cope, T., Ekman, A. M. L., and Nenes, A.: The impact of Secondary Ice Production on Arctic Stratocumulus, *Atmos. Chem. Phys.*, 20, 1301–1316, <https://doi.org/10.5194/acp-2019-804>, 2020.
- 805
- Stephens, G.L.: Radiation profiles in extended water clouds. II. Parameterization schemes. *J. Atmos. Sci.*, 35, 2123–2132, 1978
- 810 Sullivan, S.C., Lee, D., Oreopoulos, L., and Nenes, A.: The role of updraft velocity in temporal variability of cloud hydrometeor number, *Proc. Nat. Acad. Sci.*, 113, 21, 2016
- Sullivan, S. C., Kiselev, A., Leisner, T., Hoose, C., and Nenes, A.: Initiation of secondary ice production in clouds, *Atmos. Chem. Phys.*, 18, 1593–1610, doi:10.5194/acp-18-1593-2018,
- 815 2018a.
- Sullivan, S. C., Barthlott, C., Crosier, J., Zhukov, I., Nenes, A., and Hoose, C.: The effect of secondary ice production parameterization on the simulation of a cold frontal rainband, *Atmos. Chem. Phys.*, 18, 16461–16480, <https://doi.org/10.5194/acp-18-16461-2018>, 2018b.
- 820 Takahashi, T., Nagao, Y., and Koshiyama, Y.: Possible high ice particle production during graupel-graupel collisions, *J. Atmos. Sci.*, 52, 4523–4527, doi:10.1175/1520-0469, 1995.
- Vardiman, L.: The generation of secondary ice particles in clouds by crystal-crystal collision, *J. Atmos. Sci.*, 35, 2168–2180, doi:10.1175/1520-0469, 1978.
- 825
- Verlinde, J., Flatau, P.J., and Cotton, W.R.: Analytical Solutions to the Collection Growth Equation: Comparison with Approximate Methods and Application to Cloud



- Microphysics Parameterization Schemes. *J. Atmos. Sci.*, 47, 2871–2880, [https://doi.org/10.1175/1520-0469\(1990\)047<2871:ASTTCG>2.0.CO;2](https://doi.org/10.1175/1520-0469(1990)047<2871:ASTTCG>2.0.CO;2)
- 830
- Verlinde, J. and W.R. Cotton, 1993: Fitting Microphysical Observations of Nonsteady Convective Clouds to a Numerical Model: An Application of the Adjoint Technique of Data Assimilation to a Kinematic Model. *Mon. Wea. Rev.*, 121, 2776–2793, [https://doi.org/10.1175/1520-0493\(1993\)121<2776:FMOONC>2.0.CO;2](https://doi.org/10.1175/1520-0493(1993)121<2776:FMOONC>2.0.CO;2)
- 835 Vignon, É., Besic, N., Jullien, N., Gehring, J., & Berne, A. Microphysics of snowfall over coastal East Antarctica simulated by Polar WRF and observed by radar. *J. Geophys. Res.: Atmospheres*, 124, 11452–11476, 2019.
- Yano, J.-I. and Phillips, V. T. J.: Ice-ice collisions: an ice multiplication process in
840 atmospheric clouds, *J. Atmos. Sci.*, 68, 322–333, doi:10.1175/2010JAS3607.1, 2011.
- Yano, J.-I., Phillips, V. T. J., and Kanawade, V.: Explosive ice multiplication by mechanical break-up in-ice-ice collisions: a dynamical system-based study, *Q. J. Roy. Meteor. Soc.*, 142, 867–879, <https://doi.org/10.1002/qj.2687>, 2016.
- 845
- Young, G., Lachlan-Cope, T., O'Shea, S. J., Dearden, C., Listowski, C., Bower, K. N., Choularton T.W., and Gallagher M.W.: Radiative effects of secondary ice enhancement in coastal Antarctic clouds. *Geophys. Res. Lett.*, 46, 23122321, <https://doi.org/10.1029/2018GL080551>, 2019.
- 850
- 855
- 860 **Tables:**



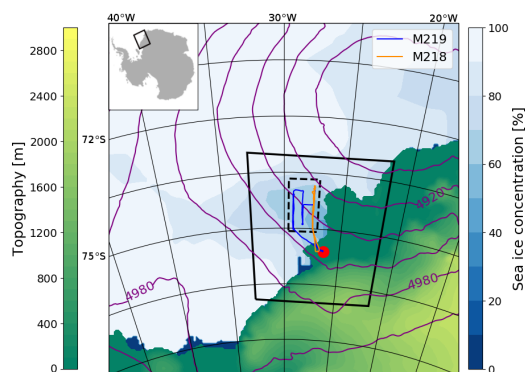
Table 1: Mean modeled downward and upward shortwave (SWD_{SFC} , SWU_{SFC}) and longwave (LWD_{SFC} , LWU_{SFC}) surface radiation, along with upward shortwave and longwave (SWU_{TOA} , LWU_{TOA}) radiation at the top of the atmosphere, during flights M218 and M219. Model results are averaged over the dashed rectangular area in Fig. 1.

Simulation	SWD_{SFC} (Wm^{-2})	SWU_{SFC} (Wm^{-2})	LWD_{SFC} (Wm^{-2})	LWU_{SFC} (Wm^{-2})	SWU_{TOA} (Wm^{-2})	LWU_{TOA} (Wm^{-2})
CNTRL	323.9	182.1	244.3	304.6	255.8	218.4
PHIL0.2	328.6	184.5	244.1	304.6	254.8	218.5
PHIL0.3	322.3	181.0	247.4	305.3	256.6	217.9
PHIL0.4	339.7	190.8	243.3	304.9	251.1	219.8
FRAG1	354.1	198.6	236.7	303.8	246.9	221.5
FRAG1siz	335.7	188.8	244.0	304.6	250.5	220.7
TAKAH	365.9	206.5	229.8	303.3	242.5	221.2
TAKAHsiz	349.5	194.5	237.0	304.2	246.6	222.0



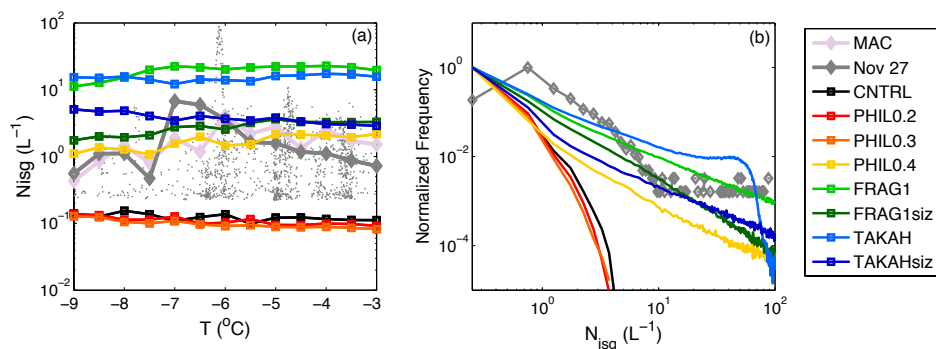
Figures:

870



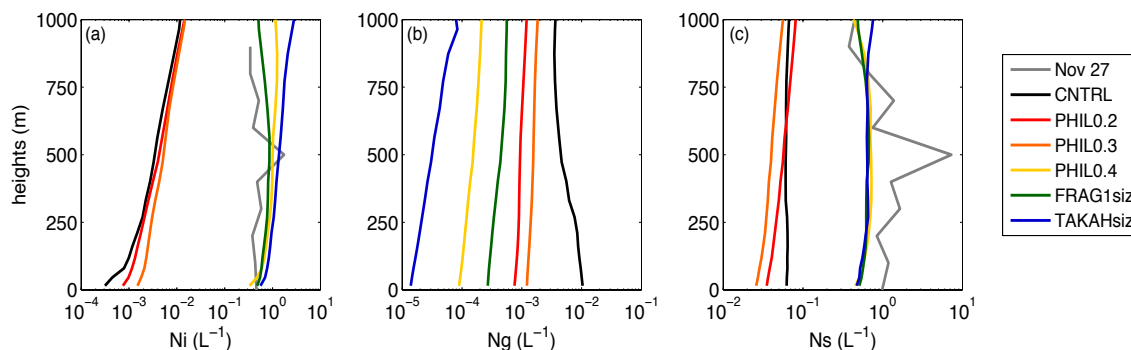
875 **Figure 1:** Map of Antarctic domains. Colors indicate terrain heights (green to yellow) and
sea-ice concentrations (blue to white), whereas the purple contours correspond to 500 hPa
geopotential heights from the CNTRL simulation at 18:00 UTC, 27 November 2015. The
black solid line delimits the 1-km horizontal grid spacing domain, while the dashed one
880 outlines the subset of the nest used for direct comparison with the aircraft data. Orange and
blue lines indicate the flight tracks, while the red circle represents Halley station. The small
figure in the top right corner indicates the location of the 1-km horizontal grid spacing domain
relative to the Antarctic continent.

885



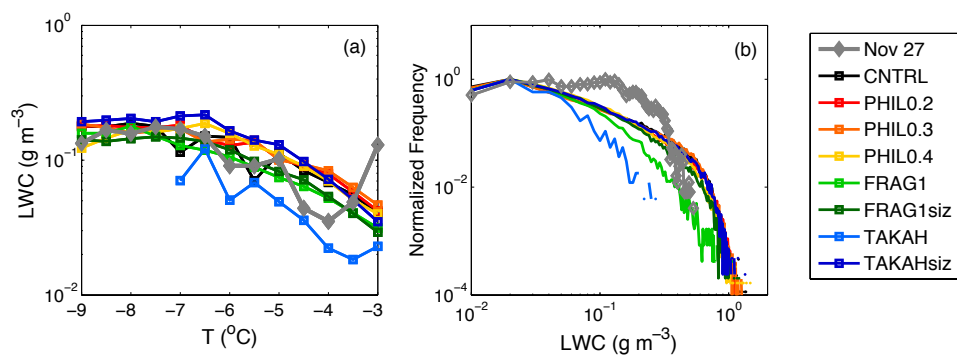
890 **Figure 2:** (a) Mean ice number concentrations (cloud ice+snow+graupel, N_{isg}) as a function
 of temperature for the whole MAC campaign (pink), our case study (grey) and the eight
 model simulations. Grey dots indicate point observations. (b) Relative frequency distribution
 of N_{isg} , binned in $0.5 L^{-1}$ intervals, scaled with maximum frequency. Ice properties are
 calculated for particles $> 80 \mu m$ and for $N_{isg} > 0.005 L^{-1}$ within the lowest 1.5 km a.s.l.

895



900 **Figure 3:** Mean vertical profiles of number concentrations of modeled (a) cloud ice, (b)
 graupel and (c) snow for six simulations. Grey lines represent measured concentrations with
 diameters (a) smaller and (c) larger than $125 \mu m$. Ice properties from the model are calculated
 for $N_{isg} > 0.005 L^{-1}$. For consistency with observations, only particles with sizes $> 80 \mu m$ are
 included in the modeled profiles in panels (a) and (c).

905



910 **Figure 4:** (a) Mean liquid water content (LWC) as a function of temperature for our case
study (grey) and the eight model simulations. (b) Relative frequency distribution of LWC,
binned in 0.01 g m^{-3} intervals, scaled with maximum frequency. Only values greater than 0.01
 g m^{-3} within the lowest 1.5 km a.s.l. are included in the analysis.

915

920

925